JACS
JOURNAL OF THE AMERICAN CHEMICAL SOCIETY

Article

pubs.acs.org/JACS

Surface Polarity and Self-Structured Nanogrooves Collaboratively Oriented Molecular Packing for High Crystallinity toward Efficient Charge Transport

Deyang Ji,[†,∥,#] Xiaomin Xu,[†,⊥,#] Longfeng Jiang,[†,#] Saeed Amirjalayer,[∥,Δ,#] Lang Jiang,[†] Yonggang Zhen,[*,†] Ye Zou,[†] Yifan Yao,[†] Huanli Dong,[†] Junsheng Yu,[§] Harald Fuchs,[∥] and Wenping Hu[*,†,‡]

[†]Key Laboratory of Organic Solids, Institute of Chemistry, Chinese Academy of Sciences, Beijing 100190, China

[‡]Tianjin Key Laboratory of Molecular Optoelectronic Sciences, Department of Chemistry, School of Science, Tianjin University & Collaborative Innovation Center of Chemical Science and Engineering (Tianjin), Tianjin 300072, China

[§]State Key Laboratory of Electronic Thin Films and Integrated Devices, School of Optoelectronic Information, University of Electronic Science and Technology of China (UESTC), Chengdu 610054, China

[∥]Center for Nanotechnology, Heisenbergstraße 11, 48149 Münster, Germany & Physikalisches Institut, Westfälische Wilhelms-Universität, Wilhelm-Klemm-Straße 10, 48149 Münster, Germany

[⊥]Department of Chemistry, The Chinese University of Hong Kong, Shatin, New Territories, Hong Kong, China

[Δ]Center for Multiscale Theory and Computation, Westfälische Wilhelms-Universität Münster, Wilhelm-Klemm-Straße 10, 48149 Münster, Germany

Supporting Information

ABSTRACT: Efficient charge transport in organic semiconductors is essential for construction of high performance optoelectronic devices. Herein, for the first time, we demonstrate that poly(amic acid) (PAA), a facilely deposited and annealing-free dielectric layer, can tailor the growth of organic semiconductor films with large area and high crystallinity toward efficient charge transport and high mobility in their thin film transistors. Pentacene is used as a model system to demonstrate the concept with mobility up to 30.6 $cm^2\ V^{-1}\ s^{-1}$, comparable to its high quality single crystal devices. The structure of PAA has corrugations with OH groups pointing out of the surface, and the presence of an amide bond further allows adjacent polymer strands to interact via hydrogen bonding, leading to a self-rippled surface perpendicular to the corrugation. On the other hand, the strong polar groups (−COOH/−CONH) of PAA could provide repulsive forces between PAA and pentacene, which results in the vertical orientation of pentacene on the dielectric surface. Indeed, in comparison with its imidized counterpart polyimide (PI), PAA dielectric significantly enhances the film crystallinity, drastically increases the domain size, and decreases the interface trap density, giving rise to superior device performance with high mobility. This concept can be extended to more organic semiconducting systems, e.g., 2,6-diphenylanthracene (DPA), tetracene, copper phthalocyanine (CuPc), and copper hexadecafluorophthalocyanine (F_{16}CuPc), demonstrating the general applicability. The results show the importance of combining surface nanogrooves with the strong polarity in orienting the molecular arrangement for high crystallinity toward efficient charge transport in organic semiconductors.

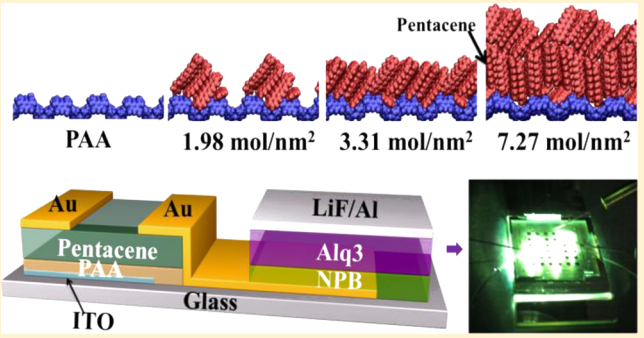

INTRODUCTION

Efficient charge transport in organic semiconductors is essential for construction of high performance organic thin film transistors (OTFTs). An appropriate gate dielectric is one of the most critical components determining the performance of a device, since the conducting channel locates at the dielectric−semiconductor interface,[1−3] which affects the growth, morphology, crystallinity, and traps of organic semiconductor.[4−8] Compared with vapor-deposited oxide dielectrics, polymer dielectrics are particularly important by possessing advantages of facile solution processability, tunable surface functionalization, and high compatibility with organic semiconductors.[9,10] However, to date, the absence of technologies to control molecular packing on polymer insulators with ideal dielectricity and facile processability has hindered OTFTs from performing

Received: November 24, 2016
Published: January 27, 2017

DOI: 10.1021/jacs.6b12153
J. Am. Chem. Soc. 2017, 139, 2734−2740

perfectly and blocked the integration of OTFTs for emerging flexible display and labeling technology.[1−3,11]

Jiang et al.[12] demonstrated that a molecular monolayer is sufficient to function as an ideal conducting channel. On silicon wafer, self-assembled monolayers (SAMs), e.g., octadecyltrichlorosilane (OTS), on a thermally grown SiO_2 dielectric work effectively to approach this target.[1,2] However, the patterning of molecules on polymer dielectrics into a desired packing arrangement within the first few molecular layers remains a bottleneck, leading to an ineffective charge transport in the polymer dielectric−organic semiconductor interface and a low mobility of corresponding OTFTs.[2]

We have been focusing on polymer dielectrics toward large area OTFT arrays and flexible circuits for years,[13−15] and have been acknowledging the challenges confronted. Here, we demonstrate substantial progress on those challenges, utilizing a polymer with strong polarity and inter-hydrogen-bonding functionality to configure polymer corrugated nanogrooves on the surface, which assist the formation of densely packed vertical molecular layers in the conducting channel to get extremely high performance OTFTs. Pentacene is used as a model system to demonstrate the concept that can be extended to other conjugated systems including tetracene, copper phthalocyanine (CuPc), 6-diphenylanthracene (DPA), and fluorinated copper phthalocyanine (F_{16}CuPc). Vertically standing pentacene molecular layers are observed at a low thickness of the thin film, demonstrating an "orthorhombic phase" which is rarely observed on a common dielectric surface.[16] In particular, the devices show a low operating voltage of −3.0 V and a high mobility up to 30.6 $cm^2\ V^{-1}\ s^{-1}$, comparable to that of high quality pentacene single crystal devices.[17] The high mobility OTFTs are further applied to drive the active-matrix organic light emitting diodes (AMOLEDs) successfully, demonstrating a general promising applicability of such a polymer dielectric toward advanced organic optoelectronics.

RESULTS AND DISCUSSION

PAA (Figure 1a), the precursor of polyimide (PI) (Figure 1b), was synthesized from pyromellitic dianhydride (PMDA) and 4,4′-oxydiphenylenediamine (ODA). Each chemical repeat unit in PAA contains carboxylic acid and amide groups, providing high solubility in various polar solvents. The ring closure is normally carried out at higher temperatures (150−300 °C), with PAA converted partially or completely into PI. The secondary structure of PAA was studied by atomistic simulations, revealing corrugations with OH groups pointing out of the surface. With the slow evaporation of the solvent, the presence of an amide bond −CONH allows adjacent polymer strands to interact strongly via hydrogen bonding while the twisted oxydiphenylene units act as the template for corrugation. Thus, a further structuring of the surface perpendicular to the corrugation can be achieved in a thermodynamic way, leading to a well-defined self-rippled PAA film (Figure 1c). In contrast to the self-assembled corrugation nanogrooves for PAA, the imidized product PI shows noncorrugation structure and the interaction between the polymer strands is mainly via weak van der Waals interactions, resulting in a flat 2D structure (Figure 1d).

According to the computation results, the differences in the secondary structure of PAA and PI have a substantial influence on the patterning ability of deposited semiconducting molecules, especially in the first few molecular layers. In the case of PAA, it is energetically favorable for pentacene

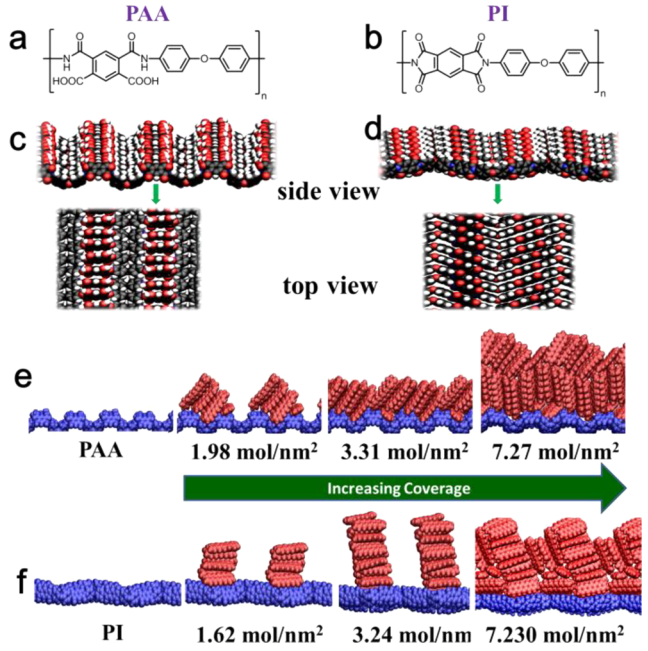

Figure 1. Molecular structures and secondary structures of PAA (a, c) and PI (b, d) (color scheme for the results of the atomistic simulations: black, carbon; red, oxygen; blue, nitrogen; white, hydrogen). Molecular orientation of pentacene molecules on PAA (e) and PI (f) with different coverages of pentacene (indicated by mol/nm^2; for clarity, the polymer is shown in blue and the pentacene molecules in red).

molecules to adhere to the corrugated nanogrooves selectively due to the strong interactions. On the basis of the "accurate positioning effect" by nanogrooves, pentacene molecular layers with the short intermolecular contacts can be aligned perpendicularly (edge-on) on the PAA surface (Figure 1e), which will be greatly beneficial for charge transport. In contrast, the PI surface, lacking such corrugated nanogrooves, does not provide a matrix for the vetical alignment of pentacene molecules. Therefore, the strong pentacene intermolecular interactions become the governing factor for molecular stacking, resulting in a random orientation in organic film as unravelled by theoretical calculation (Figure 1f).

Cho and co-workers have demonstrated that the intermolecular interactions at the interface between poly(3-hexylthiophene) (P3HT) and the polar/nonpolar functionalized SAMs ($-NH_2/-CH_3$) have a substantial effect on the preferred conformations of the P3HT chains in monolayer films.[18,19] The much stronger polarity of PAA as compared to PI was revealed by the polar component contribution to the surface energy, which was determined from the contact angle of two kinds of liquids, namely, water and diiodomethane (Table S1). For PAA with very polar carboxylic acid groups (−COOH), there is a repulsive force between the π-electron clouds of the pentacene backbone and the unshared electron pairs of oxygen atoms in the COOH-functionalized dielectric. The strong electronegativity of the two oxygen atoms in the −COOH group contributes significantly to the repulsion interactions, which drive the pentacene molecules to orient vertically with a small PAA/pentacene contact area. Further, there are two kinds of hydrogen bonding interactions between pentacene and PAA. One is between the pentacene π system and the H atoms of −COOH/−CONH groups from PAA. The other is between the H atoms of pentacene and the O/N atoms of −COOH/−

DOI: 10.1021/jacs.6b12153
J. Am. Chem. Soc. 2017, 139, 2734−2740

CONH groups from PAA. In addition, the conformation of PAA is twisted due to the ether bridge and the adjacent repulsive interactions between −COOH and −CONH groups, making it energetically unfavorable for the formation of flat-lying pentacene molecules on the PAA surface. Besides the corrugated nanogrooves, the combination of repulsive forces and hydrogen bonding interactions accounts for the vertical orientation of pentacene on the surface of PAA (Figure S1). Consequently, the stand-upright pentacene molecules aggregate into a crystal nucleus by C−H···π interactions, which further grow into large domains. In the case of PI dielectric, the imide group is much less polar relative to the carboxylic acid group. There is a relatively smaller repulsive force between the π-electron clouds of the pentacene backbone and the unshared electron pairs of the imide-functionalized PI dielectric because of weakened electronegativity of the oxygen atom in the imide group with respect to the carboxylic acid moiety. The hydrogen bonding also exists between the H atoms of pentacene and the O atoms of the imide groups for PI. It is noteworthy that the planar electron-withdrawing moieties of pyromellitic diimide display strong electron donor−acceptor interactions with electron-rich pentacene molecules. We speculate that the last factor plays a dominant role in the interactions between pentacene and PI polymer. Therefore, the random orientation of pyromellitic diimide in PI chains induces the disordered arrangement of pentacene with an amorphous state on a PI surface (Figure S1).

A nice superfine structure of corrugated nanogrooves was observed as shown in AFM images of PAA (Figure 2a), while

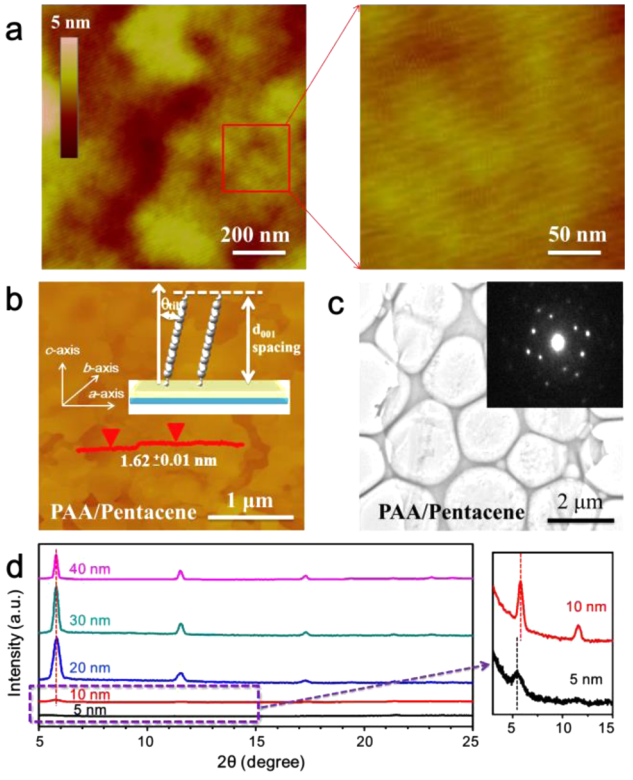

Figure 2. (a, b) AFM images of PAA and of pentacene on PAA. (c) The TEM image of pentacene thin film on PAA dielectric and its corresponding SAED pattern (inset). (d) The XRD patterns of pentacene thin films with different thicknesses grown on PAA substrate. An enlarged view of the XRD patterns of 5 and 10 nm pentacene is shown on the right.

no corrugated nanogrooves were seen on the films of PAA annealed at 180 and 300 °C (Figure S2a,b). This confirms the results of theoretical modeling (Figure 1c). Vacuum-deposited pentacene thin film on PAA showed a step height of 1.62 nm by AFM (Figure 2b), corresponding nicely to the length of the pentacene molecule.[20] This observation suggests an upright orientation of the pentacene molecules,[21,22] consistent with the theoretical modeling shown in Figure 1e. Transmission electronic microscopy (TEM) (Figure 2c) and selected area electron diffraction (SAED) patterns (inset of Figure 2c) of pentacene films on PAA exhibit ordered diffraction patterns (see also Figure S3), confirming the high crystallinity of pentacene films grown on PAA. For comparison, pentacene films deposited on PI film were also investigated, exhibiting an amorphous nature, as shown in Figure S4.

In accordance with the SAED patterns, pentacene thin films with different thicknesses (5, 10, 20, 30, and 40 nm) on PAA exhibit (00l) diffractions (Figure 2d), further indicating high crystallinity of the films. In particular, the (001) diffraction pattern peak (2θ = 5.46) at the beginning (5 nm) of the growth process yields a d_{001} spacing of 1.62 nm, which is the same as that measured from AFM, supporting the formation of an orthorhombic phase.[21] This representative peak for the orthorhombic phase at 2θ = 5.46° was not observed from pentacene films on PI, and a very weak diffraction peak at 2θ = 5.83° was observed for 20 nm film (Figure S5), indicating a rather low crystallinity with a random orientation of the pentacene molecules on the PI surface. All of the AFM, SAED, and XRD results agree well with the theoretical modeling, highlighting the importance of the corrugated nanostructure and surface polarity of the polymer surface in controlling the molecular orientation and crystallinity of the organic semiconductors.

Bottom-gate top-contact (BGTC) OTFTs were fabricated on ITO/glass substrates with a layer of PAA dielectric. For comparison, OTFTs based on PI were also fabricated under the same conditions. Vapor-deposited Au was used as source and drain electrodes. A cross-section scheme for the device structure is shown in Figure 3a. The typical transfer and output $I-V$ curves are shown in Figure 3b and c, exhibiting a field-effect mobility up to 30.6 $cm^2\ V^{-1}\ s^{-1}$ from the saturation region and ON/OFF ratio of 3×10^5 under a low operating voltage of V_{DS} = −3.0 V when the capacitance value per unit area at a frequency of 100 Hz is used. There is only a small decrease of 10.8% in the estimation of device mobility when the capacitance value at a frequency of 20 Hz is used, corroborating the outstanding device performance. To our knowledge, this result presents one of the best results of pentacene OTFTs to date.[16,23,24] A threshold voltage is lower than −0.5 V, and a subthreshold swing is about 130 mV/decade calculated from the transfer curve. This subthreshold swing yields a low interface trap density of $2.40 \times 10^{11}\ cm^{-2}$, indicating a high quality interface between the pentacene film and the PAA dielectric layer.[25] Such a high quality dielectric surface further led to low gate current leakage (Figure 3b) and negligible hysteresis, as observed between the forward and reverse sweeps (Figure S6a).

Notably, the average mobility of several tens of devices was calculated as $22.8 \pm 6.0\ cm^2\ V^{-1}\ s^{-1}$ (Figure S6b), confirming the efficient charge transport in the polymer dielectric−organic semiconductor interface among the highest values reported for OTFTs.[11,26,27] The devices well exhibited gate modulation in both the linear and saturation regimes, as shown in Figure 3d.

DOI: 10.1021/jacs.6b12153
J. Am. Chem. Soc. 2017, 139, 2734−2740

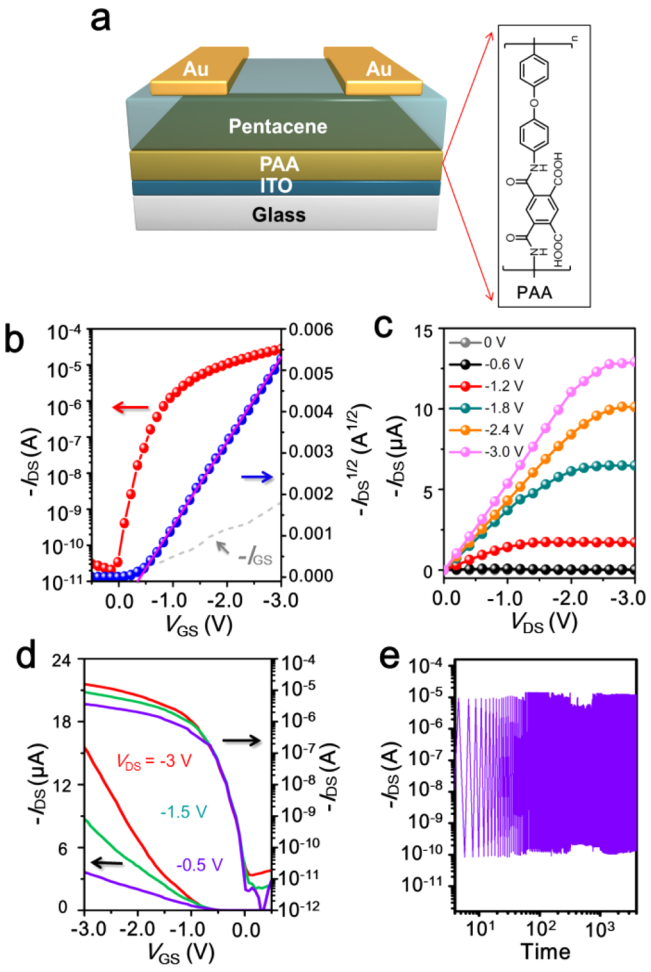

Figure 3. (a) The structure of OTFT with PAA as the insulator. (b) Typical transfer curves of the OTFT with 20 nm pentacene and a channel dimension of W = 206 μm, L = 25 μm. The gate current as a function of gate-source voltage is shown in gray. (c) Output curves of the same device at gate voltages from 0 to −3 V in 0.6 V steps. (d) Transfer curves at saturation (V_{DS} = −3 V in red) and linear region (V_{DS} = −1.5 V in blue and V_{DS} = −0.5 V in purple) of a transistor based on 20 nm pentacene on the PAA insulator. (e) The switch cycles of the drain current as a function of the cycling time.

Outstanding operating stabilities were demonstrated with on/off ratios over 10^4−10^5 and switch cycles ≥4000 cycling tests (Figure 3e). In addition, we noticed a slight decrease of device mobility after storage in an ambient environment for 60 days (Figure S6c).

Moreover, devices with different thicknesses (5−40 nm) of the active layers were studied comparatively, as shown in Figure S6d, indicating the optimum result is for 20 nm thick pentacene film. Interestingly, pentacene film as thin as 5 nm exhibited a mobility up to 11.0 $cm^2\ V^{-1}\ s^{-1}$ (Figure S6e and f), suggesting an efficient charge transport in the first few molecular layers at the dielectric/semiconductor interface.[12,28] In contrast, OTFTs based on PI dielectric exhibited very low performance with a mobility of 0.1 $cm^2\ V^{-1}\ s^{-1}$ and a threshold voltage of −2.0 V (Figure S7). The results confirm that vertical molecular alignment assisted by PAA corrugation nanogrooves and strong polarity tremendously improves charge transport, while PI cannot provide such surface nature, resulting in uncontrolled molecular packing and poor transport properties.

An integrated optoelectronic device based on OTFTs is an essential goal for organic electronics, as well as an efficient platform to identify the mobility of corresponding OTFTs. It is known that one of the main obstacles for integrated optoelectronic devices is the lack of OTFTs with sufficiently high mobility and high ON−OFF ratio to achieve a reasonable switching speed in logic circuits and to drive OLEDs, e.g., active-matrix organic light emitting diodes (AMOLEDs). As an example, here we present a simple pixel-like configuration in which OTFTs supply the current to drive the OLED arrays of 4,4′-bis (*N*-phenyl-1-naphthylamino) biphenyl (NPB) and tris(8-hydroxyquinoline) aluminum (Alq_3). The scheme of the AMOLED is shown in Figure 4a, and the OTFT arrays

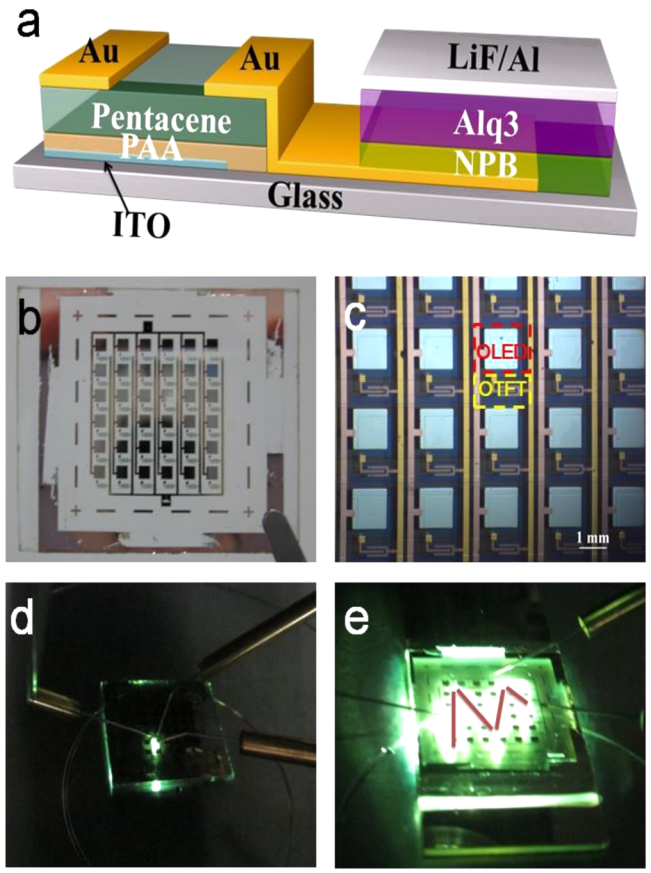

Figure 4. Structure and circuits of an active-matrix organic light emitting diode (AMOLED). (a) A configuration of OTFTs driving OLED pixel. (b) The actual picture of a large-area (2 cm × 2 cm) AMOLED. (c) An enlarged view of an AMOLED. (d) A single AMOLED display driver. (e) M-shape AMOLED display driver.

driving OLED arrays are shown in Figure 4b,c (2 cm × 2 cm transparent device arrays with 160 nm PAA, 20 nm pentacene, channel width of 8000 μm, and length of 50 μm). When an OTFT is switched on, the current flows from the source electrode to the OLED cathode, and hence, the OLED can be switched on and off by the OTFT gate voltage V_G. The switched-on single OLED and OLED arrays are shown in Figure 4d and 4e, respectively. The AMOLED successfully driven by the OTFTs confirms the high mobility of the OTFTs and the great perspective of the OTFTs for practical application.

The different performances of pentacene OTFTs based on PAA and PI dielectrics suggest the importance of chemical

DOI: 10.1021/jacs.6b12153
J. Am. Chem. Soc. 2017, 139, 2734−2740

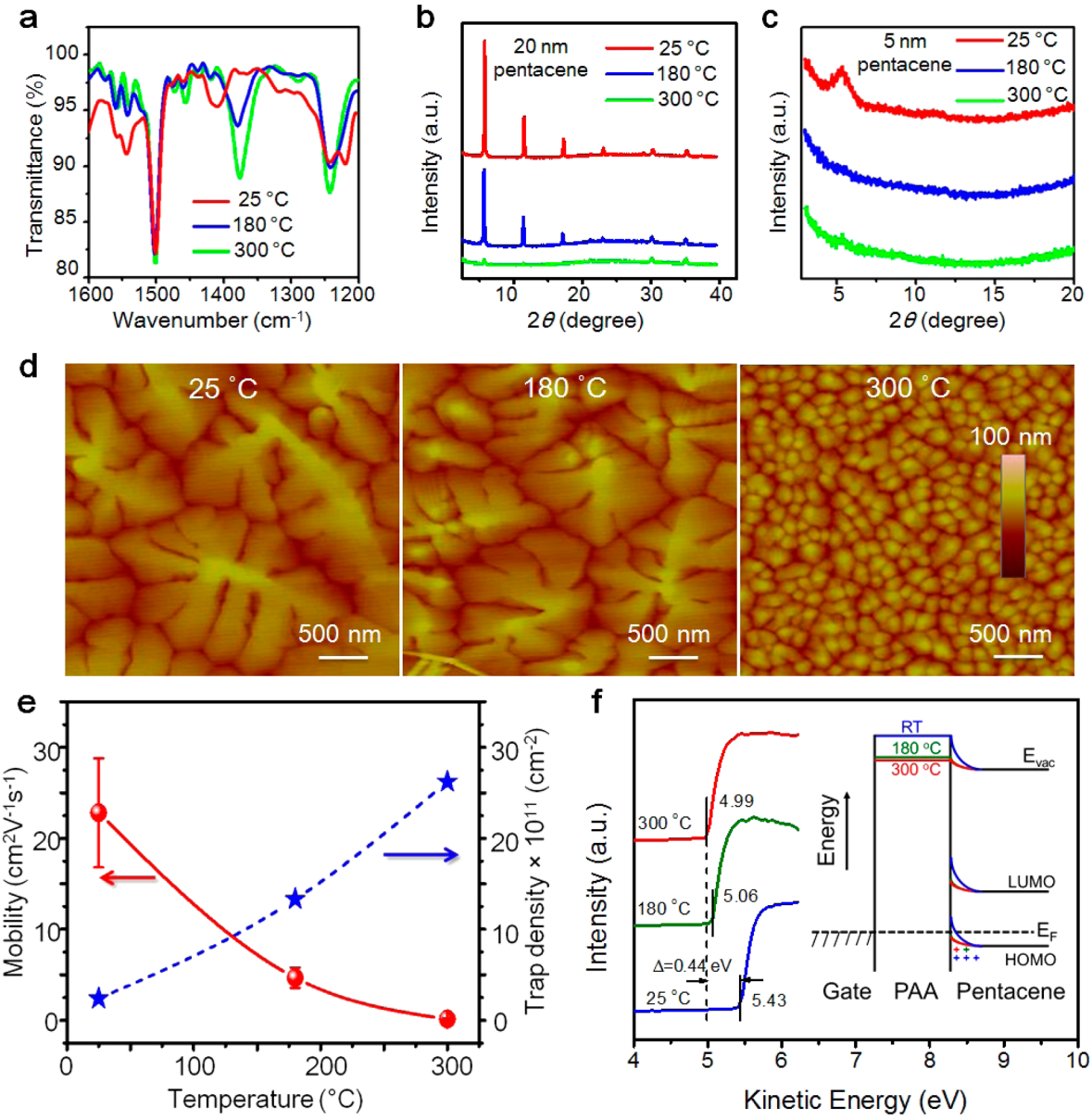

Figure 5. (a) Attenuated total reflection infrared spectroscopy (ATR) of PAA with different annealing temperatures. (b) The XRD pattern of pentacene films (20 nm) on the annealing-free PAA (25 °C, in red) surface and the imidized surface annealed at 180 °C (in blue) and 300 °C (in green), respectively. (c) The XRD pattern of pentacene (5 nm) on the annealing-free PAA (25 °C, in red) surface and the imidized surface annealed at 180 °C (in blue) and 300 °C (in green), respectively. (d) AFM images of pentacene on the annealing-free PAA (25 °C) surface and the imidized surface annealed at 180 and 300 °C, respectively. (e) The mobility and trap density as a function of temperature. (f) The UPS secondary electron emission cutoff spectra of the 5−8 nm PAA films on ITO with different annealing temperatures. The inset shows the schematic energy level diagram for the different temperature annealed-PAA/pentacene interface. HOMO, the highest occupied molecular orbital; LUMO, the lowest unoccupied molecular orbital; E_F, Fermi level energy; E_{vac}, vacuum level energy.

structure confinement of the polymer dielectrics, which has not been carefully addressed previously regardless of its importance during device fabrication. PAA, the precursor of PI, can be converted to PI through ring closure by heating. In view of a tunable degree of imidization, a systematic study was carried out with different annealing temperature treatment after formation of PAA films, i.e., pure PAA at 25 °C (annealing-free treatment), the mixture of PAA and PI obtained by annealing PAA at 180 °C, and pure PI obtained by annealing PAA at 300 °C. Attenuated total reflection infrared spectroscopy (ATR) was used to measure the degree of imidization (Figure 5a). Theoretically, the unchanged stretching vibration of the carbon−carbon double bond (C═C, 1500 cm^{-1}) of the benzene ring can be viewed as the internal standard, and thus, the degree of imidization is defined by the ratio of peak intensity of ~1375 cm^{-1} (C—N—C) and that of 1500 cm^{-1} (C═C).[29−31] When the imidization degree of PAA annealed at 300 °C (PI) is set as 100% (Figure 5a, green line), the imidization degree of PAA annealed at 180 or 25 °C is calculated as 58% (Figure 5a, blue line) or 0% (Figure 5a, red line), respectively. It is found that the crystallinity of the pentacene films is highly dependent on the dielectric imidization degree (Figure 5b). The highest crystallinity of pentacene film was observed on the surface of 0% imidized PAA, while the lowest crystallinity was observed when PAA was completely converted into PI.

DOI: 10.1021/jacs.6b12153
J. Am. Chem. Soc. 2017, 139, 2734−2740

More importantly, a predominating orthorhombic crystal phase occurred in the preliminary growth of pentacene (5 nm) on PAA, while an amorphous state was observed in the cases with PAA annealed at 180 and 300 °C (Figure 5c). The thin film morphology of pentacene also varied substantially with different annealing treaments of PAA. As monitored by AFM, the average grain size of pentacene was around 2.5 μm on an annealing-free (25 °C) PAA dielectric, and it decreased to 100 nm on top of the film annealed at 300 °C (Figure 5d). On the basis of the above results, the growth model of pentacene films on PAA at different annealing temperatures was illustrated in Figure S8. At an annealing-free temperature of 25 °C, pentacene molecules grow vertically on the dielectric layer with the orthorhombic phase in the first few layers. On the other hand, pentacene molecules aggregate disorderly with a high annealing temperature of 180 or 300 °C, resulting in a low degree of packing order. The maximum interface trap density deduced from the transfer curves under each imidization condition (Figure 5e) indicates that the higher degree of imidization gives rise to the higher interface trap density and the lower device performance. Furthermore, the work function of annealing-free PAA is relatively higher than that of PAA annealed at 180 and 300 °C, as shown in Figure 5f. Consequently, the band bending at the PAA dielectric/pentacene interface shifts toward higher energy (inset of Figure 5f), leading to a higher hole density on the insulator surface in the channel.[32,33] Thus, the pentacene TFT using a PAA dielectric layer shows a far superior field-effect mobility. This observation also suggests that electrons from the pentacene film are extracted by PAA, leaving behind more mobile holes in the conductive channel, and a more positive gate bias is needed to turn off the device.[32,33] It is obvious that the finely tuned surface nature of PAA provides pentacene films with high crystallinity, large domain size, and low trap density, all of which account for efficient charge transport. On the other hand, poor crystallinity, small domain size, and high trap density presented in the partially or fully imidized surfaces (PI) constrain significantly carrier migration, thus leading to poor charge mobility.

Ultimately, in order to confirm the general applicability, PAA was extended to OTFTs based on other organic semiconductors, e.g., 2, 6-diphenylanthracene (DPA), tetracene, copper phthalocyanine (CuPc), and copper hexadecafluorophthalocyanine (F_{16}CuPc) with the performances listed in Figure S9. The superior device performance based on PAA with respect to their counterpart devices on PI suggests that PAA can be used as an excellent dielectric layer featuring good compatibility with organic semiconductors.

CONCLUSION

In summary, we demonstrate that polymer dielectric nanogroove structure and polarity could assist vertical molecular alignment of organic semiconductors toward efficient charge transport in a dielectric−semiconductor interface. Particularly, the PAA dielectric with OH groups pointing out of the surface allows adjacent polymer strands to interact via hydrogen bond, leading to a self-rippled surface with corrugated nanogrooves, which induce pentacene molecules to stand upright. Besides that, the very polar carboxylic acid group of PAA provides the pronounced repulsive forces between PAA and pentacene, further driving pentacene molecules to orient vertically with a small PAA/pentacene contact area. Indeed, PAA films significantly induce the generation of the pentacene orthorhombic phase, enhance the film crystallinity, increase the domain size, and decrease the interface trap density in comparison with their imidized counterpart PI, thus leading to efficient charge transport and far superior device performance. Moreover, PAA demonstrates its general applicability for other organic semiconductors, showing high compatibility and wide applicability toward organic optoelectronics.

ASSOCIATED CONTENT

Supporting Information

The Supporting Information is available free of charge on the ACS Publications website at DOI: 10.1021/jacs.6b12153.

OTFT characteristics, AFM, TEM, and SAED images, and electrical and optical characteristics of PAA dielectric (PDF)

AUTHOR INFORMATION

Corresponding Authors

*zhenyg@iccas.ac.cn

*huwp@tju.edu.cn

ORCID

Saeed Amirjalayer: 0000-0003-0777-5004

Junsheng Yu: 0000-0002-7484-8114

Wenping Hu: 0000-0001-5686-2740

Author Contributions

#D.J., X.X., L.J., S.A.: These authors contributed equally to this work.

Notes

The authors declare no competing financial interest.

ACKNOWLEDGMENTS

The authors are grateful to Prof. Eiichi Nakamura (The University of Tokyo), Prof. Dezhen Wu (Beijing University of Chemical Technology), Prof. Christopher R. McNeill (Monash University, Australia), Prof. Qian Miao (the Chinese University of Hong Kong), and Prof. Liqiang Li (The Suzhou Institute of Nano-tech and Nano-bionics, CAS) for insightful discussion. They sincerely thank Dr. Jie Liu for transmission spectroscopy measurement, Dr. Zongrui Wang for AFM analysis, and Dr. Xiaolong Fu for preparation of device figures. They acknowledge financial support from the Ministry of Science and Technology of China (2016YFB04001100, 2014CB643600, 2013CB933403, 2013CB933500), National Natural Science Foundation of China (51633006, 91233205, 91222203, 51303185), and the Strategic Priority Research Program of the Chinese Academy of Sciences (XDB12000000).

REFERENCES

(1) Bao, Z. N.; Locklin, J. *Organic Field-Effect Transistors*; CRC Press: New York, 2007.

(2) Hu, W. *Organic Optoelectronics*; Wiley-VCH: Weinheim, Germany, 2012.

(3) Voss, D. *Nature* **2000**, *407*, 442.

(4) Facchetti, A.; Yoon, M. H.; Marks, T. *Adv. Mater.* **2005**, *17*, 1705.

(5) Kim, C.; Facchetti, A.; Marks, T. *Adv. Mater.* **2007**, *19*, 2561.

(6) Kim, C.; Facchetti, A.; Marks, T. *Science* **2007**, *318*, 76.

(7) Wang, C.; Lee, W. Y.; Nakajima, R.; Mei, J. G.; Kim, D. H.; Bao, Z. *Chem. Mater.* **2013**, *25*, 4806.

(8) Diao, Y.; Tee, B. C-K.; Giri, G.; Xu, J.; Kim, D. H.; Becerril, H. A.; Stoltenberg, R. M.; Lee, T. H.; Xue, G.; Mannsfeld, S. C. B.; Bao, Z. *Nat. Mater.* **2013**, *12*, 665.

DOI: 10.1021/jacs.6b12153
J. Am. Chem. Soc. 2017, 139, 2734−2740

(9) Gelinck, G. H.; Huitema, H. E. A.; Veenendaal, E. V.; Cantatore, E.; Schrijnemakers, L.; Putten, J. B. P. H. V.; Geuns, T. C. T.; Beenhakkers, M.; Giesbers, J. B.; Huisman, B.; Meijer, E. J.; Benito, E. M.; Touwslager, F. J.; Marsman, A. W.; Rens, B. J. E. V.; Deleeuw, D. M. *Nat. Mater.* **2004**, *3*, 106.
(10) Moon, H.; Seong, H.; Shin, W. C.; Park, W.; Kim, M.; Lee, S.; Bong, J. H.; Noh, Y.; Cho, B. J.; Yoo, S.; Im, S. G. *Nat. Mater.* **2015**, *14*, 628.
(11) Yuan, Y.; Giri, G.; Ayzner, A. L.; Zoombelt, A. P.; Mannsfeld, S. C. B.; Chen, J.; Nordlund, D.; Toney, M. F.; Huang, J.; Bao, Z. *Nat. Commun.* **2014**, *5*, 3005.
(12) Jiang, L.; Dong, H.; Meng, Q.; Li, H.; He, M.; Wei, Z.; He, Y.; Hu, W. *Adv. Mater.* **2011**, *23*, 2059.
(13) Ji, D.; Jiang, L.; Cai, X.; Dong, H.; Meng, Q.; Tian, G.; Wu, D.; Li, J.; Hu, W. *Org. Electron.* **2013**, *14*, 2528.
(14) Ji, D.; Jiang, L.; Guo, Y.; Dong, H.; Wang, J.; Chen, H.; Meng, Q.; Fu, X.; Tian, G.; Wu, D.; Yu, G.; Liu, Y.; Hu, W. *Adv. Funct. Mater.* **2014**, *24*, 3783.
(15) Ji, D.; Jiang, L.; Dong, H.; Zhen, Y.; Meng, Q.; Hu, W. *J. Mater. Chem. C* **2014**, *2*, 4142.
(16) Wang, C. H.; Hsieh, C. Y.; Hwang, J. C. *Adv. Mater.* **2011**, *23*, 1630.
(17) Jurchescu, O. D.; Popinciuc, M.; van Wees, B. J.; Palstra, T. T. M. *Adv. Mater.* **2007**, *19*, 688.
(18) Kim, D. H.; Jang, Y.; Park, Y. D.; Cho, K. *Langmuir* **2005**, *21*, 3203−3206.
(19) Kim, D. H.; Park, Y. D.; Jang, Y.; Yang, H.; Kim, Y. H.; Han, J. I.; Moon, D. G.; Park, S.; Chang, T.; Chang, C.; Joo, M.; Ryu, C. Y.; Cho, K. *Adv. Funct. Mater.* **2005**, *15*, 77−82.
(20) Mattheus, C. C.; de Wijs, G. A.; de Groot, R. A.; Palstra, T. T. M. *J. Am. Chem. Soc.* **2003**, *125*, 6323.
(21) Cheng, H.; Mai, Y.; Chou, W.; Chang, L.; Liang, X. *Adv. Funct. Mater.* **2007**, *17*, 3639.
(22) Fritz, S. E.; Martin, S. M.; Frisbie, C. D.; Ward, M. D.; Toney, M. F. *J. Am. Chem. Soc.* **2004**, *126*, 4084.
(23) Chou, W.; Kuo, C.; Chang, C.; Yeh, B.; Chang, M. *J. Mater. Chem.* **2010**, *20*, 5474.
(24) Sun, X.; Zhang, L.; Di, C.; Wen, Y.; Guo, Y.; Zhao, Y.; Yu, G.; Liu, Y. *Adv. Mater.* **2011**, *23*, 3128.
(25) Yoon, M.; Kim, C.; Facchetti, A.; Marks, T. J. *J. Am. Chem. Soc.* **2006**, *128*, 12851.
(26) Minemawari, H.; Yamada, T.; Matsui, H.; Tsutsumi, J.; Haas, S.; Chiba, R.; Kumai, R.; Hasegawa, T. *Nature* **2011**, *475*, 364.
(27) Tseng, H.; Phan, H.; Luo, C.; Wang, M.; Perez, L. A.; Patel, S. N.; Ying, L.; Kramer, E. J.; Nguyen, T.; Bazan, G. C.; Heeger, A. J. *Adv. Mater.* **2014**, *26*, 2993.
(28) Cao, Q.; Kim, H.; Pimparkar, N.; Kulkarni, J. P.; Wang, C.; Shim, M.; Roy, K.; Alam, M. A.; Rogers, J. A. *Nature* **2008**, *454*, 495.
(29) Suzuki, Y.; Maekawa, Y.; Yoshida, M.; Maeyama, K.; Yonezawa, N. *Chem. Mater.* **2002**, *14*, 4186.
(30) Han, E.; Wu, D.; Qi, S.; Tian, G.; Niu, H.; Shang, G.; Yan, X.; Yang, X. *ACS Appl. Mater. Interfaces* **2012**, *4*, 2583.
(31) Han, E.; Wang, Y.; Chen, X.; Shang, G.; Yu, W.; Niu, H.; Qi, S.; Wu, D.; Jin, R. *ACS Appl. Mater. Interfaces* **2013**, *5*, 4293.
(32) Pernstich, K. P.; Haas, S.; Oberhoff, D.; Goldmann, C.; Gundlach, D. J.; Batlogg, B.; Rashid, A. N.; Schitter, G. *J. Appl. Phys.* **2004**, *96*, 6431.
(33) Jang, Y.; Cho, J. H.; Kim, D. H.; Park, Y. D.; Hwang, M.; Cho, K. *Appl. Phys. Lett.* **2007**, *90*, 132104.

DOI: 10.1021/jacs.6b12153
J. Am. Chem. Soc. 2017, 139, 2734−2740